Proteome-wide analysis of mutant p53 targets in breast cancer identifies new levels of gain-of-function that influence PARP, PCNA, and MCM4

Alla Polotskaia[a], Gu Xiao[a], Katherine Reynoso[a], Che Martin[a], Wei-Gang Qiu[a], Ronald C. Hendrickson[b], and Jill Bargonetti[a,1]

[a]Department of Biological Sciences, Hunter College, City University of New York, New York, NY 10065; and [b]Proteomics Core Facility, Memorial Sloan–Kettering Cancer Center, New York, NY 10065

Edited* by Carol Prives, Columbia University, New York, NY, and approved January 21, 2015 (received for review August 25, 2014)

The gain-of-function mutant p53 (mtp53) transcriptome has been studied, but, to date, no detailed analysis of the mtp53-associated proteome has been described. We coupled cell fractionation with stable isotope labeling with amino acids in cell culture (SILAC) and inducible knockdown of endogenous mtp53 to determine the mtp53-driven proteome. Our fractionation data highlight the underappreciated biology that missense mtp53 proteins R273H, R280K, and L194F are tightly associated with chromatin. Using SILAC coupled to tandem MS, we identified that R273H mtp53 expression in MDA-MB-468 breast cancer cells up- and down-regulated multiple proteins and metabolic pathways. Here we provide the data set obtained from sequencing 73,154 peptide pairs that then corresponded to 3,010 proteins detected under reciprocal labeling conditions. Importantly, the high impact regulated targets included the previously identified transcriptionally regulated mevalonate pathway proteins but also identified two new levels of mtp53 protein regulation for nontranscriptional targets. Interestingly, mtp53 depletion profoundly influenced poly(ADP ribose) polymerase 1 (PARP1) localization, with increased cytoplasmic and decreased chromatin-associated protein. An enzymatic PARP shift occurred with high mtp53 expression, resulting in increased poly-ADP-ribosylated proteins in the nucleus. Mtp53 increased the level of proliferating cell nuclear antigen (PCNA) and minichromosome maintenance 4 (MCM4) proteins without changing the amount of *pcna* and *mcm4* transcripts. Pathway enrichment analysis ranked the DNA replication pathway above the cholesterol biosynthesis pathway as a R273H mtp53 activated proteomic target. Knowledge of the proteome diversity driven by mtp53 suggests that DNA replication and repair pathways are major targets of mtp53 and highlights consideration of combination chemotherapeutic strategies targeting cholesterol biosynthesis and PARP inhibition.

mutant p53 | proteome | chromatin | PARP | MCM4

The cellular response to mutations in the *p53* gene and to stable expression of mutant p53 (mtp53) protein in breast cancer is increasingly accepted as an oncogenic signal transducer (1–6). The Cancer Genome Atlas Project identified *TP53* mutations in 12% of luminal A, 32% of luminal B, 84% of basal-like, and 75% of HER2-expressing breast cancers (6). This high percentage of tumor protein p53 gene (*TP53*) mutations across all subtypes of breast cancers indicates the high significance of mtp53 expression and harkens back to the original identification of p53 as a proto-oncogene (7). Many *TP53* mutations are missense changes that cause a change in a single amino acid residue most often found in the central site-specific DNA binding domain, but the mutations cause variable changes that range from loss to gain of function (2, 4). Although some *TP53* mutations contribute to breast cancer metastasis because of loss of p53 tumor suppressor activity, many missense *TP53* mutations cause newfound gain-of-function oncogenic activities to the mtp53 protein that range from activation of tumor-promoting target genes to the inhibition of p53 family members p63 and p73 (5). This gain of function is associated with mtp53 protein that often has a prolonged $t_{1/2}$ and is highly expressed in cancer cells (8, 9). The predominant mode of mtp53-mediated regulation has been described as activation and repression of gene transcription (2, 4, 5, 10).

Primary "hotspot" residues for mutation in the p53 393-aa protein found in human cancers are R175, G245, R248, R249, R273, and R282 (2, 4, 5). Mouse models knocked in for expressing the mtp53 equivalents to human R175H and R273H demonstrate gain of function (compared with mice without p53, or with WT p53) by displaying more metastatic tumors (11, 12). However, it remains unclear how these different mutations result in altered signal transduction that causes increased tumorigenesis and metastasis. One commonly proposed mechanism is that mtp53 proteins are recruited to DNA by other sequence-specific DNA-binding transcription factors and modify the transcription of growth-activating target genes. One example is mtp53 R273H, which activates transcription of the cholesterol biosynthesis genes through interaction with the sterol regulatory element-binding protein (SREBP) family of transcription factors (3). Muller and Vousden have suggested that mtp53 gain of function changes cellular programming by multiple mechanisms (2). These mechanisms include alteration in the DNA-binding ability of

Significance

Mutant p53 (mtp53) is a driver oncogene of breast cancer. Here, for the first time, to our knowledge, using an inducible endogenous knockdown system, we explore the mtp53 driven proteome. We report this key data set that highlights mtp53-driven proteome diversity at the level of protein localization, as well as changes in protein levels without corresponding changes in transcription. We validated two protein pathways that include increased chromatin association of poly(ADP ribose) polymerase 1, and the increase of nuclear replication proteins minichromosome maintenance 4 and proliferating cell nuclear antigen. The addition of mtp53 proteomic targets to the previously identified transcriptional targets suggests that effective treatment of mtp53-driven breast cancers may be facilitated by new combination protocols blocking proteins of the metabolic pathways of cholesterol biosynthesis, DNA replication, and DNA repair.

Author contributions: A.P. and J.B. designed research; A.P., G.X., K.R., R.C.H., and J.B. performed research; C.M., W.-G.Q., and J.B. contributed new reagents/analytic tools; A.P., G.X., C.M., W.-G.Q., R.C.H., and J.B. analyzed data; and A.P., G.X., and J.B. wrote the paper.

The authors declare no conflict of interest.

*This Direct Submission article had a prearranged editor.

Freely available online through the PNAS open access option.

[1]To whom correspondence should be addressed. Email: bargonetti@genectr.hunter.cuny.edu.

This article contains supporting information online at www.pnas.org/lookup/suppl/doi:10.1073/pnas.1416318112/-/DCSupplemental.

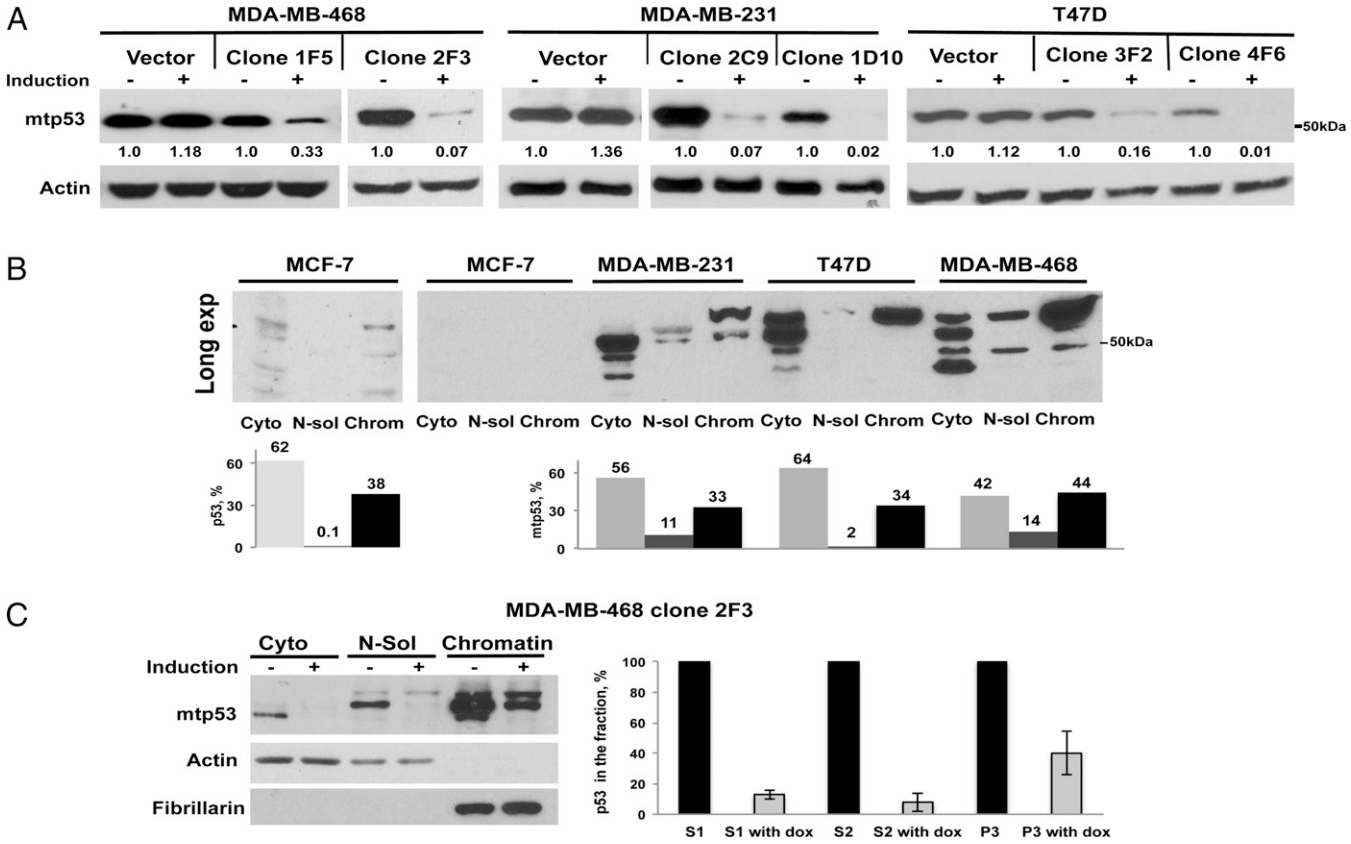

Fig. 1. Inducible depletion of mtp53 proteins R273H, R280K, and L194F in breast cancer cell lines shows they are efficiently depleted in the cytoplasm and strongly associated with chromatin. (*A*) The mtp53 expression in whole-cell extract from vector controls and clones MDA-468.shp53 1F5 and 2F3, MDA-231. shp53 2C9 and 1D10, and T47D.shp53 3F2 and 4F6 is shown. Cells were grown in the presence or absence of doxycycline (4 μg/mL for T47D and 8 μg/mL for other cell lines) for 6 d. Whole-cell lysates were prepared as described in *Materials and Methods*, and 50 μg of protein was separated by gradient 4–12% SDS/PAGE and analyzed by Western blot using antibody to p53. Actin was used as a loading control. Relative depletion of mtp53 was quantified by ImageJ analysis. (*B*) Biochemical fractionation of MCF-7, MDA-MB-231, T47D, and MDA-MB-468 breast cancer cells was carried out according to the well-established method of Méndez and Stillman (23). The cytoplasmic, nuclear-soluble, and chromatin-enriched protein samples were resolved in a gradient 4–12% SDS/PAGE in amounts proportional to the subcellular fraction of 100 μg of protein derived from a cell pellet. The p53 subcellular localization was determined by immunoblotting. ImageJ was used to quantify the percent distribution. (*C*) Biochemical fractionation of MDA-468.shp53 2F3 clone was carried out with or without p53 depletion. Fractions were run with 50 μg of protein loaded per lane and normalized for actin in the cytoplasmic and nuclear-soluble fractions and fibrillarin in the chromatin-enriched fraction. ImageJ was used to quantify the values. The Western blot is a representative image for doxycycline knockdown for 12 d, and the histogram is a mean (SD) of two independent experiments.

mtp53, causing direct regulation of new targets; another involves interactions of mtp53 with multiple transcription factors or other DNA-binding proteins, thus resulting in activation of some genes and repression of others. The latter proposes that the interaction of mtp53 with some proteins might regulate an enzymatic activity that is not involved in gene regulation. Interestingly, preferential binding of hotspot mutants has been detected on supercoiled DNA, suggesting a conformational recognition pathway (13). Therefore, multiple approaches could be used to therapeutically target the oncogenic mtp53 pathway (10). The study of mtp53-driven outcomes on the cancer cell proteome has the potential to determine signal transduction targets for which pharmacological protein inhibitors or activators could be designed.

Surprisingly, to date, we are aware of no study that has reported what global influence an endogenous gain-of-function mtp53 has on a cancer cell proteome. The gain-of-function mtp53 R273H global influence on the transcriptome enlightened our understanding of multiple pathways influenced by mtp53, and these included the up-regulation of genes in the cell division, cell cycle, and sterol biosynthesis pathways (3). Two proteomic studies for mtp53-driven changes have examined mtp53-interacting proteins in cancer cells and embryonic stem cells using whole cell lysates and have identified factors that regulate cancer cell invasion and reversion of conformational mtp53 to WT p53 structure and function, respectively (14, 15).

Improved detection of proteomic signal transduction changes are observed with subcellular fractionation experiments of stable isotope labeling with amino acids in cell culture (SILAC) followed by liquid chromatography (LC) and tandem MS (LC-MS/MS) (16, 17). One such study identified poly(ADP ribose) polymerase (PARP) as a critical chromatin-associated factor, which is recruited to DNA damage sites to block transcription and facilitate DNA repair. We used a similar approach to focus on how mtp53 influences the breast cancer cell proteome. To dissect this, we combined inducible mtp53 depletion with cell fractionation and quantitative MS. Through these coordinated methodologies, we discovered that gain-of-function mtp53 regulates protein targets through two previously unidentified nontranscriptional pathways. We found that R273H mtp53 targets PARP to the chromatin, and increases the amount of chromatin-associated proliferating cell nuclear antigen (PCNA) and minichromosome maintenance (MCM) 4 (MCM4) without changing *pcna* or *mcm4* transcription. Moreover, when mtp53 is depleted, PARP protein and enzymatic activity shift to the cytoplasm. This new knowledge sets the stage for more direct targeting of proteins driven by gain-of-function mtp53 in breast cancers. It suggests that combination

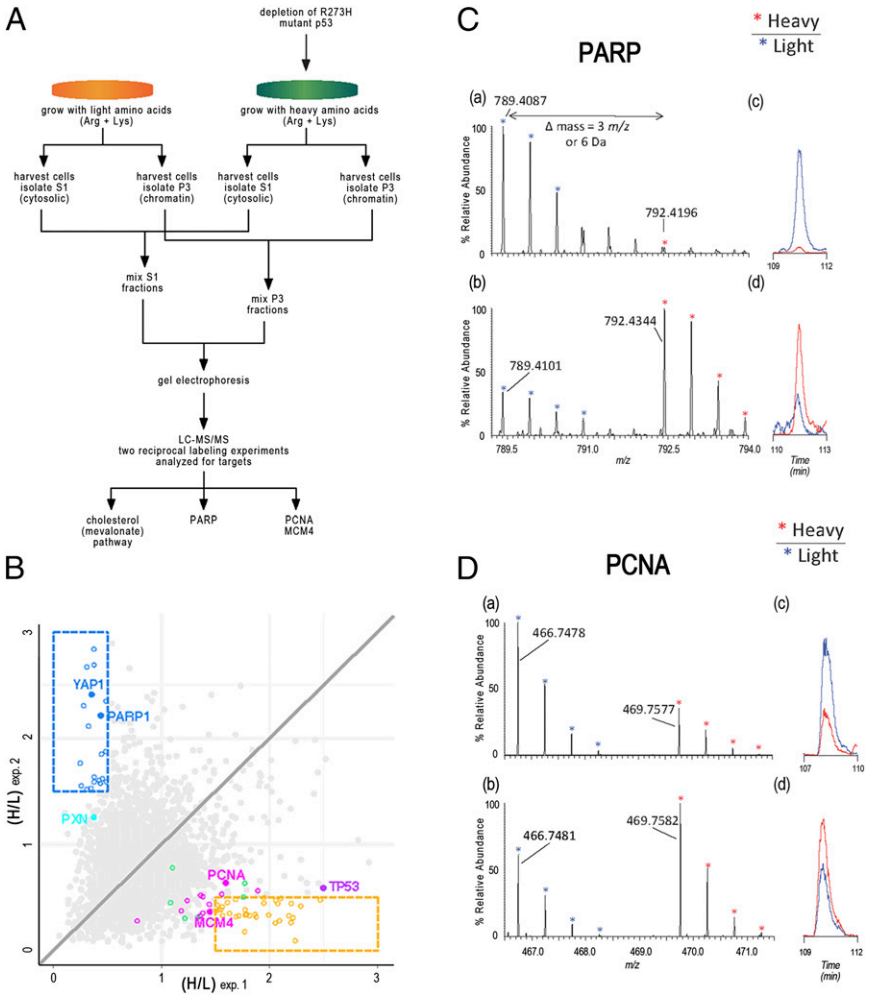

Fig. 2. Proteomics screen of stable isotope-labeled cells in culture (SILAC) determines multiple mtp53 targets and regulated pathways. (*A*) Overview of the proteomics strategy to determine mtp53 targets in MDA-MB-468 cells. (*B*) mtp53 depleted and untreated cytoplasmic fraction from MDA-468.shp53 2F3 were mixed from cells grown in heavy (labeled "H") vs. light (labeled "L") media. Normalized LC-MS/MS H/L ratios of 3,010 proteins identified from forward-labeled (*y* axis for p53 depletion in cells grown in heavy media) and reverse-labeled (*x* axis for p53 depletion in cells grown in light media) experiments were plotted. An H/L ratio > 1 or < 1 indicates an mtp53-dependent change in the amount of a protein in the cytoplasmic fraction. The diagonal line indicates a lack of change in the H/L ratio between the two experiments, which corresponds to nontarget proteins (those with H/L ratios close to 1 in both experiments) or proteins inconsistently expressed between the two experiments (those with H/L > 2 or H/L < 1 in both experiments). Targets with reciprocal H/L ratios greater than 1.5 and less than 0.5 (blue and yellow dots) have changed strongly and consistently between the depleted and untreated cells. The change in p53 (purple dot) is labeled TP53 as the positive control. The cholesterol biosynthesis enzymes are shown as green dots. The DNA replication proteins are shown as pink dots (PCNA and MCM4 are labeled), and PARP1 is one of the labeled blue dots. (*C*) Reverse labeling of R273H depletion shows high-quality LC-MS/MS peptides for PARP in the chromatin fraction. Representative MS spectra from PARP in the chromatin fraction is shown with forward and reverse labeling in *a* and *b*, respectively. The selected ion current chromatograms for the $(M+2H)^{2+}$ ions from tryptic peptide IAPPEAPVTGYMFGK at the selected retention time (109–113 min) for the forward and reverse labeling are shown in *c* and *d*, respectively. The light isoform with *m/z* 789.4 is shown in blue, and heavy isoform with *m/z* 792.4 is shown in red. The integrated area under the curve was used to calculate the change in abundance. (*D*) Representative MS spectra from PCNA in the chromatin fraction is shown with forward and reverse labeling in *a* and *b*, respectively. The selected ion current chromatograms for the $(M+2H)^{2+}$ ions from tryptic peptide YLNFFTK at the selected retention time (107–112 min) for the forward and reverse labeling are shown in *c* and *d*, respectively. The light isoform with *m/z* 466.7 is shown in blue, and heavy isoform with *m/z* 469.7 is shown in red. The integrated area under the curve was used to calculate the change in abundance.

therapeutics to block cholesterol biosynthesis, DNA replication, and DNA repair pathways may be useful for R273H mtp53-driven breast cancers.

Results

The mtp53 Proteins R273H, R280K, and L194F Are Associated with the Chromatin and Are Efficiently Depleted in the Cytoplasm. We engineered human breast cancer clones with inducible knockdown of mtp53 in the MDA-MB-468 cell line with the missense mutation R273H, the MDA-MB-231 cell line with R280K, and the T47D clones with the depletion of mtp53 L194F (Fig. 1*A*) (3, 18, 19). The p53 mutation R273H is one of the most recurrent p53 missense hotspot mutations and is therefore excellent for gain-of-function studies (2, 20). The MDA-468.shp53 R273H depletion clone 1F5 was used in work reporting mtp53-driven mevalonate pathway regulation (3), and we subsequently isolated a more efficient knockdown of mtp53 R273H in the MDA-MB-468 cell line called 2F3 (Fig. 1*A*). The 2F3 MDA-468.shp53 clone is used herein to study the R273H-driven breast cancer-associated proteome.

Since 1991, it has been accepted that mtp53 does not bind sequence-specifically to DNA (21). Moreover, it has long been established that many missense mtp53 proteins demonstrate a dominant-negative inhibition of the sequence-specific DNA binding ability of WT p53 (22). What is less widely appreciated is

that, in growing cells with overexpression of oncogenic mtp53, the mtp53 protein is tethered to the chromatin through nonspecific DNA binding activity or recruitment by other DNA binding proteins. We compared MDA-MB-468, MDA-MB-231, and T47D cells for the percentage of mtp53 associated with the chromatin (Fig. 1*B*). We carried out cell fractionation by using the well-established method from the Stillman laboratory that has been used for a number experiments using SILAC (16, 17, 23). By using this fractionation method, and running the sample so it reflected the distribution of proteins from the cell pellet, we detected that more than 30% of the mtp53 was tightly tethered to the chromatin (Fig. 1*B*). Whereas we observed that whole-cell extracts produced a single migrating p53 species (Fig. 1*A*), the cell fractionation samples resulted in multiple differentially migrating p53 proteins that may represent changes in posttranslational modifications (Fig. 1*B*). The chromatin-associated mtp53 consistently produced a species of higher molecular weight.

To determine the efficiency of R273H mtp53 removal, we compared induced knockdown and untreated 2F3 MDA-468.shp53 cell fractions (this time comparing equal amounts of total protein per lane). The efficiency of depletion of mtp53 was, on average, 90% in the cytoplasmic fraction but only 60% in the chromatin fraction (Fig. 1*C*). We have evidence that the chromatin-associated mtp53 in our cell line set is most tightly associated in MDA-468.shp53 cells. In MDA-231.shp53 and T47D.shp53 cells, the mtp53 on the chromatin was also tightly tethered, but the depletion was more efficient than seen for MDA-468.shp53 (compare Fig. S1 vs. Fig. 1*C*). All three cell lines, MDA-468.shp53, MDA-231.shp53, and T47D.shp53, showed excellent depletion of mtp53 in the cytoplasm. We used the cytoplasmic fraction of the MDA-468.shp53 2F3 clone for the SILAC global identification studies, followed by high-throughput identification of peptides by MS (Fig. 2*B*).

Stable Isotope Labeling with Amino Acids in Cell Culture Identifies mtp53-Driven Changes in Proteomic Pathways, Including DNA Replication, PARP, and Mevalonate Enzymes. SILAC of fractionated extracts has been used to identify important players in multiple cellular pathways (16, 17) but has yet to be described as a means to dissect the signal transduction pathway of oncogenic mtp53 (14). To survey the breast cancer proteome to determine factors influenced by oncogenic mtp53 R273H, we combined SILAC and cell fractionation of MDA-468.shp53 cells with inducible mtp53 depletion (Fig. 2*A* shows workflow). High-throughput identification of peptides by MS was used to compare depletion vs. nondepletion conditions in reciprocal heavy amino acid [$^{13}C_6$,$^{15}N_4$]-arginine and [$^{13}C_6$]-lysine or light arginine and lysine to differentially label the depletion vs. nondepletion conditions. For reciprocal labeling and validation, we carried out forward and reverse labeling with depletion of the R273H mtp53 in the heavy labeled conditions for one sample set and depletion of R273H under the light amino acid incorporation conditions for the other sample set. MDA-468.shp53 with R273H depleted and nondepleted cells were harvested and fractionated, and the cytoplasmic fractions (or chromatin) were mixed at a 1:1 ratio of cells grown with heavy or light amino acids. The mixed fractions were separated by SDS/PAGE, digested by trypsin, and analyzed by LC-MS/MS (Fig. 2*A*). We were able to determine the relative abundance of light and heavy peptides in the R273H depleted vs. nondepleted conditions. A total of 73,154 peptide pairs from the cytoplasmic fraction were sequenced, corresponding to 4,248 proteins. Forward and reverse labeling in the two variable conditions allowed confident annotation of changing pathways in response to R273H knockdown. We determined the relative abundance of each protein under the two conditions and calculated the median heavy:light (H/L) ratio from the corresponding peptide pairs by using MaxQuant. There were 3,010 proteins that were detected under the reciprocal conditions, and these proteins were graphed for the H/L ratio Cartesian coordinates for the two experiments (Fig. 2*B*). In the graph, median ratios > 1 on the *x* axis and < 1 on the *y* axis identify a protein that is high when R273H p53 is high. As a SILAC-positive control, we show the p53 H/L ratio Cartesian coordinate (Fig. 2*B*, labeled purple spot TP53). It was previously determined that R273H activates transcription of the cholesterol biosynthesis target genes (3). Importantly, we recovered six enzymes of the cholesterol biosynthesis pathway in the proteomic screen, and they are shown in green in Fig. 2*B*. An interactive map for all the reciprocal hits shown in Fig. 2*B* is provided at diverge.hunter.cuny.edu/Polotskaia_etal_2014/supp-fig-s1/. Moreover, there were many high-stringency peptides in the forward and reverse labeling experiments that showed a H/L ratio greater than 1.5 for one set and less than 0.5 for the reciprocal set (Fig. 2*B*, blue and yellow boxed spots). These peptides were categorized as highly relevant. Importantly, the protein PARP1 was one of these targets (Fig. 2*B*, labeled blue spot in upper left quadrant). PARP1 catalyzes the transfer of ADP ribose to target proteins and plays a role in many cellular processes, including transcription, DNA replication, and DNA repair (24, 25). PARP1 and two other R273H mtp53 notable protein targets in the left quadrant (Fig. 2*B*) were Yes-associated protein 1 (YAP1) and Paxillin (PXN), and these were validated as changing in the MDA-468.shp53 2F3 cell line by Western blot analysis (Fig. S2 shows MDA-MB-468 cells). Interestingly, these differences were most striking for R273H-dependent outcomes and were not exemplified for the other two mtp53 proteins tested (Fig. S2).

Genome-wide expression analysis of the reciprocal cytoplasmic proteomic targets identified gene pathways that were up-regulated and down-regulated by R273H mtp53 (Fig. 2*B*; see also data set available at diverge.hunter.cuny.edu/Polotskaia_etal_2014/supp-table-s1/). The full outputs of the Gene Set Enrichment Analysis (GSEA; version 2.0.14) (26) are available at diverge.hunter.cuny.edu/Polotskaia_etal_2014/supp-table-s1/. To view up-regulated pathways and genes, click the link marked as "Detailed enrichment results in html format" under the first "Enrichment in phenotype" heading, which will lead to a list of up-regulated pathways. For each listed pathway, clicking the "GS Details" column leads to a table of genes associated with the pathway. The first three pathways up-regulated by mtp53 included cell cycle, mitotic, and DNA replication pathways (Fig. 2*B*, pink dots and two highlighted proteins, PCNA and MCM4). One of the critical proteins found in all three up-regulated pathways was PCNA. The total set of 3,010 proteins was ranked by their $\log_2[(H/L)_{exp1}/(H/L)_{exp2}]$ ratios, with proteins changing insignificantly or inconsistently ranked close to 0 and proteins changing significantly and consistently ranked in the two extremes. The cholesterol biosynthesis pathway was the forth protein pathway that demonstrated up-regulation by mtp53 (Fig. 2*B*, green dots, lower right quadrant). As validation, all 16 genes in the cholesterol biosynthesis pathway were up-regulated as protein (significantly and consistently) by the mtp53 R273H in the two experiments (see data set available at diverge.hunter.cuny.edu/Polotskaia_etal_2014/supp-table-s1/, gene enrichment pathway). The gene set enrichment analysis was performed using the GSEA Preranked test in GSEA software (version 2.0.14) (26), with pathways defined by the Reactome Pathway Database (version 4.0) (27).

Depletion of mtp53 R273H Modulates PARP Localization and PARP Enzymatic Activity. PARP family enzymes are critical for a number of biological processes, including regulating transcription, DNA replication, and DNA repair. Moreover, PARP catalyzes the transfer of ADP ribose to target proteins. Interestingly, we observed through SILAC experiments that the depletion of mtp53 in MDA-468.shp53 cells increased the level of PARP1 in the cytoplasmic fraction (Fig. 2*B*) and decreased the level of PARP1 in the chromatin fraction (Fig. 2*C*). The LC-MS/MS

high-quality data and the reduction of PARP in the nuclear fraction was exemplified by examining the $(M+3H)^{3+}$ ions for the relative H/L abundance of *m/z* for PARP1 (Fig. 2*C*). The MS data also demonstrated that depletion of mtp53 correlated with a reduction of PCNA in the cytoplasmic and chromatin fractions (Fig. 2 *B* and *D*).

The PARP protein intracellular modulation by mtp53 depletion was reproducibly validated by Western blot analysis (Fig. 3*A*). This suggested that depletion of R273H p53 modulated intracellular PARP1 enzymatic activity. To test this possibility, we used immunofluorescence confocal microscopy to compare total ADP ribosylated proteins in 2F3 MDA-468.shp53 cells vs. control cells with just vector expression under induced doxycycline conditions. Importantly, we observed that, whereas mock depletion conditions (and up-regulation of GFP) had no influence on poly-ADP-ribosylated (PAR) proteins, the depletion of R273H p53 decreased the level of nuclear ribosylated proteins and increased the level of cytoplasmic ribosylated proteins (Fig. 3*B*, *Top*, representative image). Interestingly, this observation was stronger when cells were maintained in serum-deprivation conditions.

Mutant p53 Stabilizes Chromatin-Associated PCNA and MCM4. We detected that PCNA protein was up-regulated by R273H mtp53 in the cytoplasmic and nuclear fractions (Fig. 2). Our pathway analysis showed that PCNA and MCM4 proteins were up-regulated mtp53 targets listed in the DNA replication pathway (Fig. 2*B*; see also data set available at diverge.hunter.cuny.edu/Polotskaia_etal_2014/supp-table-s1/). We examined the chromatin fraction by Western blot analysis to determine just how profoundly the depletion of R273H mtp53 influenced the chromatin association of MCM4 and PCNA (Fig. 4). The depletion of R273H caused a decrease in the overall MCM4 and PCNA associated with the chromatin (Fig. 4 *A* and *B*). Global mRNA analysis and quantitative RT-PCR showed that neither of these genes had reduced transcript level (3) (Fig. 4*D*). We also showed that, whereas the depletion of mtp53 slowed the proliferation of MDA-468.shp53 cells, it did not change the overall cell cycle distribution of growing cells, indicating no concurrent growth arrest (Fig. 4*C*). To address if R280K mtp53 had a similar influence to R273H, we analyzed the chromatin fraction of MDA-231.shp53 cells after knockdown for changes in MCM4 and PCNA (Fig. 4*E*). Following R280K knockdown, neither MCM4 nor PCNA was significantly reduced. This supports data from many laboratories that different p53 mutations cause differing outcomes (4).

To determine the specificity of R273H for modulation of MCM4 and PARP in another cell line, we used siRNA-mediated knockdown in the colon adenocarcinoma cell line HT-29. Depletion of R273H mtp53 in HT-29 cells resulted in a decrease in MCM4 protein in all cell fractions (Fig. 4*F*). Importantly, we again observed that it was difficult to knock down the chromatin-associated R273H mtp53. This incomplete knockdown of R273H in HT-29 did not influence the PARP on the chromatin (Fig. S3*A*). We also tested an additional MDA-468.*shp53* clone 1F5 and again found it very difficult to deplete R273H mtp53 from the chromatin (Fig. S3*B*), and we were unable to detect a release of PARP.

Use of PARP Inhibitors to Target Breast Cancer Cells Expressing Mutant p53. To detect if PARP activity was directly promoting cell viability, we tested the efficacy of PARP inhibition for killing the breast cancer cells expressing mtp53. We used rucaparib, as it has shown promise and has been tested in some clinical trials (28–30), on the MDA-468.shp53 cells with or without mtp53 depletion (Fig. 5*A*). The knockdown of mtp53 reduced cell viability without rucaparib treatment, but the drug sensitivity was maintained (Fig. 5*B*). When normalizing cells for starting viability, the cells expressing mtp53 were slightly more sensitive to

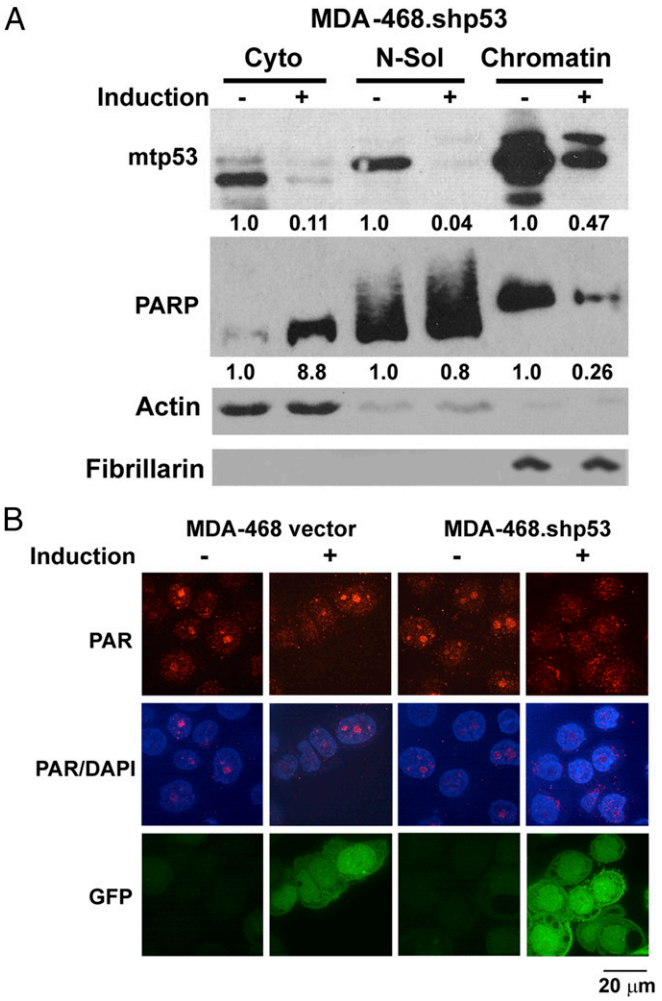

Fig. 3. Depletion of mtp53 modulates PARP localization and PARP enzymatic activity. (*A*) Cells MDA-468 vector and MDA-468.shp53 were grown in the presence or absence of 8 μg of doxycycline for 6 d, and fractionation was carried out as described. Samples were resolved on a gradient 4–12% SDS/PAGE. Protein levels of p53, PARP1, Actin, and Fibrillarin in the fractions were determined by Western blot analysis. Actin was used to normalize the cytoplasmic and nuclear-soluble fractions, and fibrillarin was used to normalize the chromatin fraction. A total of 50 μg of protein from the cytoplasmic fraction and nuclear-soluble fractions per lane and 5 μg of the chromatin fraction per lane were resolved. ImageJ was used to quantify p53 and PARP1 change in each fraction compared with the corresponding control. (*B*) Confocal microscopy images of PAR proteins were obtained by using anti-PAR antibody. DAPI staining was used to determine the nucleus, and GFP was an indicator of doxycycline-mediated induction. Images are representative of three independent experiments.

rucaparib treatment, but both populations of cells died in response to the drug (Fig. 5*C*). These data suggest that the expression of mtp53 may make cells synthetically lethal to the inhibition of PARP activity and that treating cells expressing mtp53 with PARP inhibitors may be highly efficacious.

To validate that the changes in PARP upon R273H mtp53 knockdown were not just a result of decreased cell viability, we treated the cells with a p53-independent cell death inducer. We previously showed that 8-amino-adenosine (8AA) can induce p53-independent cell death of breast cancer cell lines including MDA-MB-468 (31). We treated MDA-MB-468 cells with 8AA and measured a viability of 55% survival (Fig. 6*A*). The fractionated cell extract of the 8AA-treated cells showed no change in their

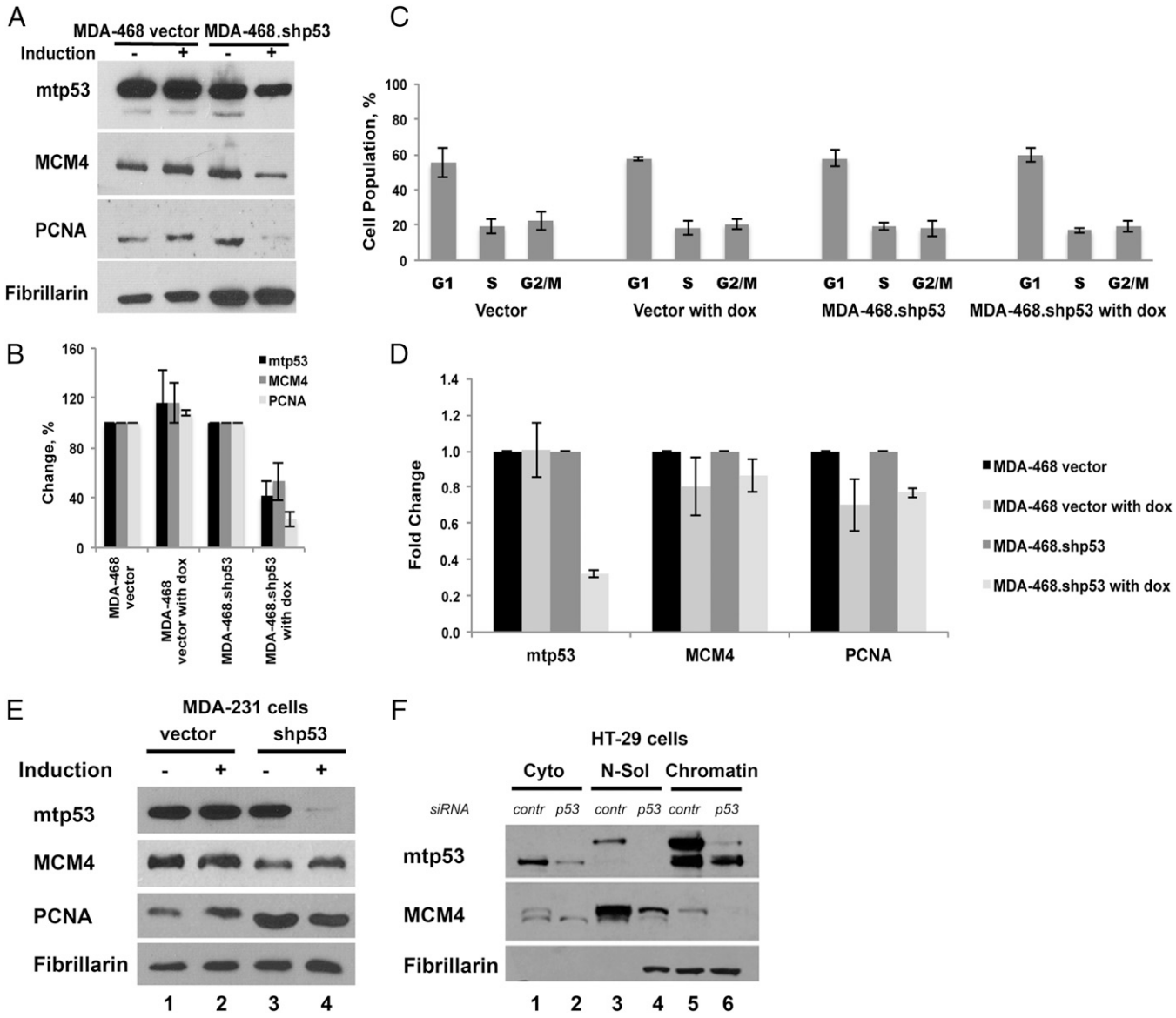

Fig. 4. Mutant p53 stabilizes chromatin-associated MCM4 and PCNA. (*A*) MDA-468 vector and MDA-468.shp53 cells were grown in the presence or absence of 8 μg of doxycycline for 12 d, and fractionation was carried out as described. A total of 50 μg of protein from the chromatin fraction was resolved in a 10% SDS/PAGE. Protein levels of mtp53, MCM4, PCNA, and Fibrillarin were determined by Western blot analysis. Fibrillarin was used to normalize the chromatin fraction. The Western blot is a representative image, and the histogram (*B*) represents the average (SD) of three independent experiments. (*C*) Knockdown of the mtp53 and decrease in MCM4 and PCNA protein levels did not change the cell cycle profile, which was analyzed by flow cytometry. Results are the mean (SD) of two independent experiments. (*D*) Quantitative PCR analysis of MCM4 and PCNA RNA levels in the MDA-468 vector and MDA-468.shp53 cells grown with or without 8 μg/mL of doxycycline were not influenced by mtp53 depletion. Results are the mean (SD) of two independent experiments. (*E*) MDA-231 vector and MDA-231.shp53 1D10 clone cells were grown in the presence or absence of 8 μg of doxycycline for 6 d, and fractionation was carried out as described. A total of 50 μg of protein from the chromatin fraction was resolved in a 10% SDS/PAGE. Protein levels of mtp53, MCM4, PCNA, and Fibrillarin were determined by Western blot analysis. (*F*) HT-29 colon cancer cells were transfected with p53-siRNA (p53) or control siRNA (contr). Biochemical fractionation was carried out after 72 h of transfection. A total of 50 μg of protein from cytoplasmic (Cyto), nuclear-soluble (N-Sol), and chromatin fractions were run per lane, and protein levels of mtp53, MCM4, and Fibrillarin in the fractions were determined by Western blot analysis.

localization or levels of PARP, MCM4, and PCNA expression (Fig. 6 *B* and *C*).

Discussion

With the use of inducible knockdown of mtp53, in conjunction with cell fractionation and SILAC, we identified R273H mtp53 proteomic targets that highlight two new levels of mtp53-target protein regulation that are not directly driven by changes in transcription (Figs. 2–4). Numerous peptides were identified by using a reciprocal SILAC screening approach, and the identified proteins were further stratified into enriched pathway components found in the cytoplasm (see map and data set available at diverge.hunter.cuny.edu/Polotskaia_etal_2014/supp-fig-s1/ and diverge.hunter.cuny.edu/Polotskaia_etal_2014/supp-table-s1/, respectively). We previously collaborated in a study showing that mtp53 R273H in MDA-MB-468 cells up-regulates the transcription of mevalonate pathway genes through an interaction with the SREBP family of transcription factors (3); here we demonstrate that R273H causes increased production of enzymes of the cholesterol biosynthesis pathway. In addition to the production of cholesterol biosynthesis enzymes, we also determined that R273H mtp53 up-regulated DNA replication proteins, including MCM4 and PCNA,

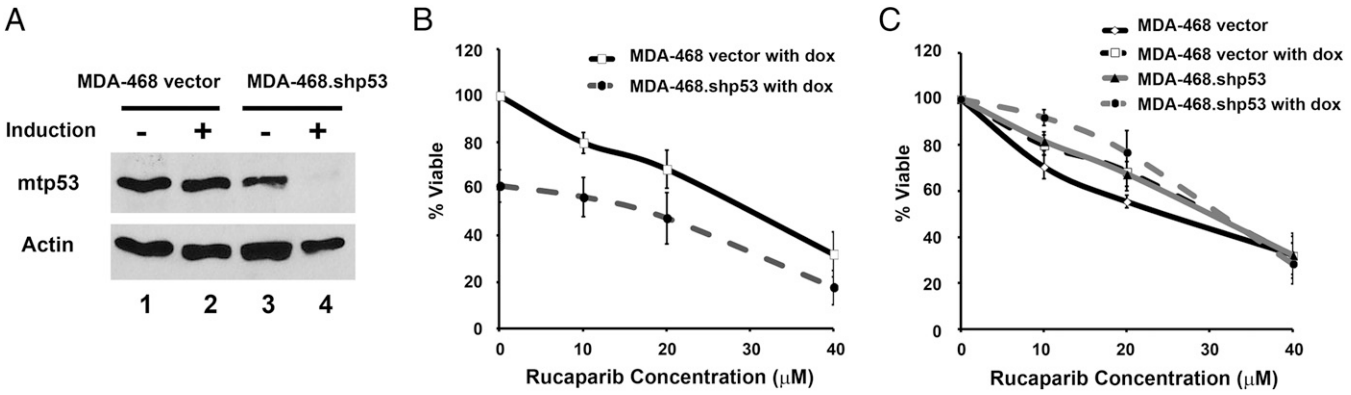

Fig. 5. Reduced cell viability of mtp53 R273H-expressing cells when PARP is pharmacologically inhibited. MDA-468.shp53 or control vector-expressing cells were treated with 8 μg/mL doxycycline (DOX) for 7 d to induce shRNA expression or left without doxycycline treatment. (*A*) Whole-cell extracts were analyzed by Western blotting for p53 depletion. Actin was used as a loading control. (*B*) MDA-MB-468 cell lines with *p53*.shRNA or control vector were treated with 8 μg/mL doxycycline (DOX) for 5 d to induce shRNA expression or left without doxycycline treatment, followed by treatment with 0, 10, 20, or 40 μM rucaparib for 48 h. A total of 100,000 cells per well were plated on the 12-well plate for cell viability 3-(4,5-dimethylthiazol-2-yl)-2,5-diphenyltetrazolium bromide (MTT) assay based on mitochondrial dehydrogenase activity (as in ref. 31). (*C*) Rucaparib reduced cell viability of MDA-468.shp53 cells in a dose-dependent fashion. Error bars indicate the SDs of two independent experiments.

without increasing the corresponding mRNA levels (Figs. 2 and 4). Interestingly, R273H mtp53 also modulated PARP1 cellular localization and enzymatic outcomes (Figs. 2 and 3). With good chromatin depletion of mtp53 R273H, the chromatin localized PARP1 was reduced and relocalized to the cytoplasm. The cytoplasmic localization of PARP1 coordinated with increased cytoplasmic PAR proteins. Taken together, our findings indicate that the signal transduction from R273H mtp53 can modulate intracellular localization of PARP and increased protein levels of key DNA replication proteins PCNA and MCMs.

It has been described that different mutations in p53 can lead to variable outcomes (4). In keeping with this fact, we saw that, whereas R273H mtp53 regulated cytoplasmic PARP, YAP, and paxillin, the mtp53 proteins R280K and L194F in MDA-231.shp53 and T47D.shp53, respectively, did not have the same outcomes (Fig. S2). Moreover, R273H was tightly tethered to the chromatin in breast cancer and colon cancer cells. We observed that R273H in HT-29 colon cancer cells also increased the level of MCM4 protein. However, tightly associated R273H with the chromatin may have been responsible for no mtp53-mediated change in PARP in HT-29 cells. It remains to be determined if there are overlapping proteomic pathways that are regulated by the mtp53 proteins differentially in different subtypes of cancers. However, our data strongly support previous reports that different hotspot mutants of p53 have different functions. Importantly, the influence of R273H strongly modifies the levels of many proteins in the MDA-MB-468 cell line and the HT-29 cell line.

Cell fractionation in conjunction with R273H mtp53 depletion enabled us to dissect variability in chromatin and cytoplasmic outcomes implicating R273H mtp53 in influencing DNA repair and DNA replication through signal transduction that did not require direct transcriptional changes to the identified targets. It has been underappreciated that mtp53 is tightly associated with chromatin even though mtp53 has lost its sequence-specific DNA binding ability. We found that R273H, R280K, and L194F mtp53 proteins were all highly associated with the chromatin

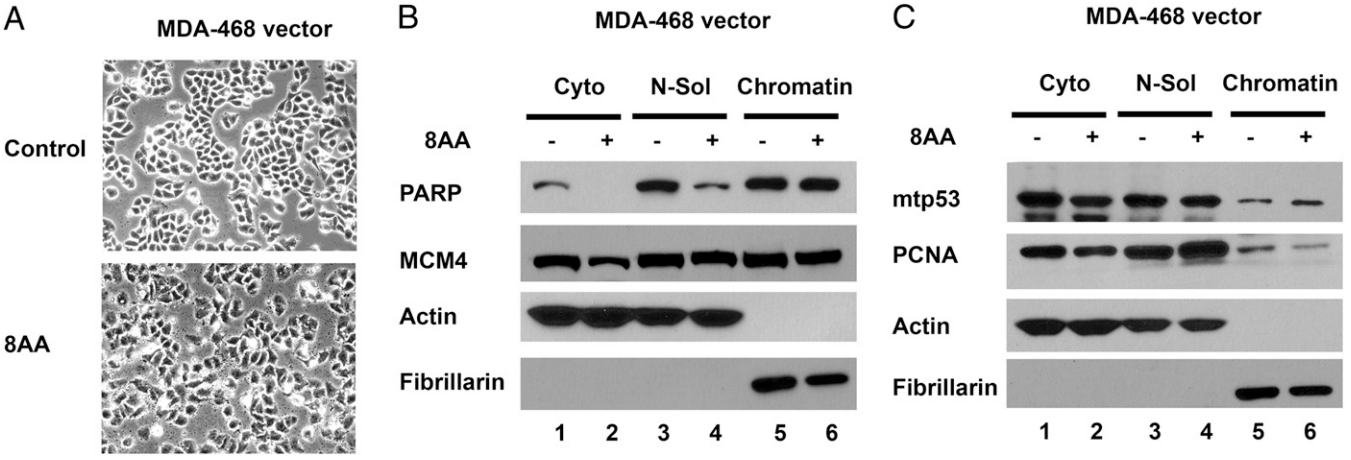

Fig. 6. 8AA-induced cell death in MDA-468 cells does not have the same proteome change as p53 depletion. (*A*) MDA-468 vector cells were left untreated (control) or treated with 15 μM of 8AA for 16 h. Phase-contrast microscopy image of cells untreated or treated with 8AA at a magnification of 20×. MDA-468 vector cells were left untreated or treated with 15 μM of 8AA for 16 h and were fractionated into cytoplasmic (cyto), nuclear-soluble (N-Sol), and chromatin fractions. (*B*) Fractions were run with 50 μg of protein loaded per lane, and protein levels of PARP1, MCM4, Actin, and Fibrillarin in the fractions were determined by Western blot analysis. (*C*) Fractions were run with 50 μg of protein from the cytoplasmic and nuclear-soluble fractions and 5 μg of the chromatin fraction, and protein levels of mtp53, PCNA, Actin, and Fibrillarin in the fractions were determined by Western blot analysis.

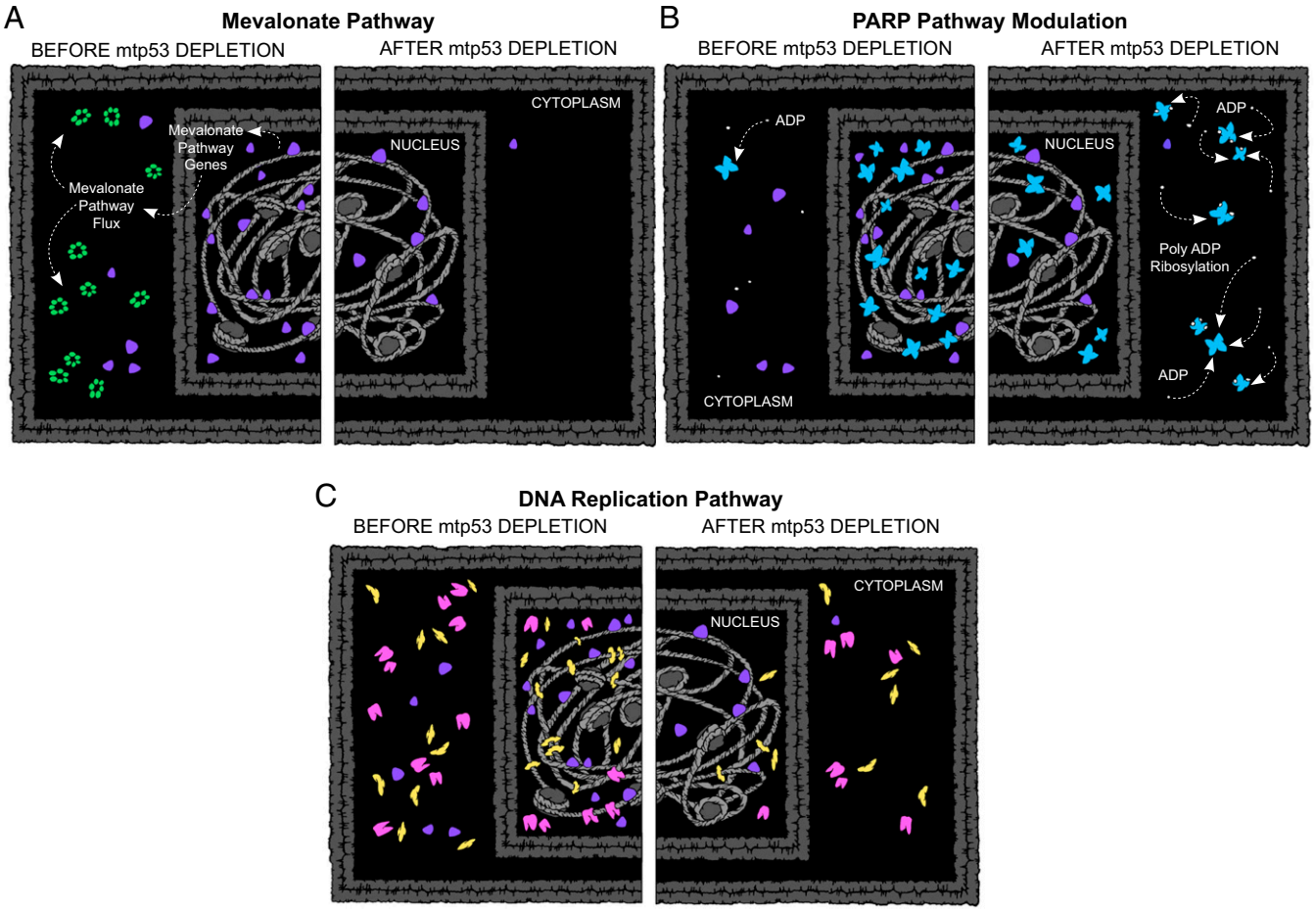

Fig. 7. Mutant p53 drives proteome changes with and without directly activating the transcription of the target. (*A*) Mevalonate pathway enzymes (green) were detected at high levels in the cytoplasm when R273H mtp53 protein levels (purple) were high, and, upon mtp53 depletion, these mevalonate protein enzymes were reduced. (*B*) PARP1 protein level (blue) was high in the nucleus when R273H mtp53 protein levels (purple) were high, and, upon mtp53 depletion, PARP1 nuclear protein levels were reduced and the cytoplasmic PARP1 was increased. The depletion of R273H mtp53 also coordinated a decrease in PAR proteins in the nucleus and an increase of PAR proteins in the cytoplasm. (*C*) PCNA and MCM4 protein levels (pink and yellow) were high when R273H mtp53 protein levels (purple) were high, and, upon mtp53 depletion, PCNA and MCM4 protein levels were reduced.

(Fig. 1 and Fig. S1). Although much of the gain-of-function activity of mtp53 has been proposed to be through modulation of transcription, presumably by functioning as a transcription cofactor, to our knowledge, no study has yet determined a specific DNA binding site for mtp53. Our data show that R273H mtp53 is tightly associated with the chromatin and can modulate the protein level and cellular localization of enzymes involved in DNA repair and DNA replication. We found that chromatin-associated R273H mtp53 was very difficult to deplete, suggesting that it remained associated with the DNA during replication. The shift in PARP1 protein and enzymatic activity following R273H mtp53 depletion was seen as a relocalization of PARP from the chromatin to the cytoplasm. This suggests that R273H mtp53 drives changes in chromatin conformation and is not just a passive chromatin partner. A detailed study of the chromatin-associated proteins that change with and without different mtp53 proteins should help to elucidate if mtp53 proteins can remodel chromatin and the protein factors involved. PARP is known to associate with cruciform and non-B DNA structures while participating in DNA repair (25, 32). Moreover, the association of PARP with chromatin is regulated by AMPK, and this influences PARP posttranslational modification (25). Therefore, our data implicate mtp53 as influencing DNA repair while possibly driving the chromatin into structures that are non-B and may include mechanisms that regulate kinase cascades. This coordinated regulation of DNA structure impinging on PARP activity has the potential to promote genomic instability that results in mtp53-associated catastrophic DNA rearrangements (i.e., chromothripsis). Mutant p53 is known to promote chromothripsis and changes overall chromosome structures (33). The relocalization of PARP following R273H mtp53 depletion suggests that cytoplasmic PARP is a cell cycle checkpoint signal, and this could become a mechanism to target cancers that express high levels of mtp53. Treating the cells with the PARP inhibitor rucaparib demonstrated a potential synthetic lethal combination for R273H mtp53 expression and PARP inhibition (Fig. 5).

An illustration of our findings for how R273H mtp53 influences the cancer cell proteome is shown in Fig. 7. A dynamic regulation of proteomic factors is depicted in colors that represent mtp53 (Fig. 7 *A*–*C*, purple), mevalonate pathway enzymes (Fig. 7*A*, green), PARP pathway modulation (Fig. 7*B*, blue), and the DNA replication enzymes MCM4 and PCNA (Fig. 7*C*, yellow and pink). The up-regulation of DNA replication components by mtp53 suggests that mtp53 directly activates cell proliferation through modulating protein amount and chromatin association of DNA replication factors. The increase in protein level did not require activation of transcription, as indicated by the fact that R273H mtp53 increased PCNA and MCM proteins but did not increase their mRNA level. This increase in PCNA and MCM4 was visible in the cytoplasm and on the chromatin.

We observed coordinated chromatin associated R273H mtp53, PCNA, MCM4, and PARP. PARP is known to poly-ADP-ribosylate proteins on chromatin to regulate DNA repair processes (25). PARP1 is activated by DNA breaks and recruits proteins that are critical in base excision repair/single strand break repair (SSBR), for example, XRCC1 (34). PARP and PCNA are both proteins that are recruited as part of the SSBR pathway (25). The recruitment of PARP and PCNA to DNA breaks disables these repair molecules from participating in repair elsewhere. Therefore, the possibility exists that mtp53 drives recruitment of PARP, MCM4, and PCNA to an altered structured chromatin and that this negatively regulates DNA repair while allowing for increased DNA replication.

Our study sheds light on the multiple roles of gain-of-function mtp53. We showed that mtp53-driven proteomic changes are not simply a result of changes in transcription of mtp53 target genes and that mtp53 causes changes in protein levels and protein localization without always directly regulating the transcription of the target. The chromatin eviction of PARP1 by mtp53 depletion suggests that one role for gain-of-function mtp53 is to stabilize chromatin-associated factors and that this may sequester proteins from carrying out their normal function and drive them to perform a function that promotes tumorigenesis. Furthermore, mtp53 increased the association of MCM4 and PCNA with the chromatin, which may increase rereplication that can drive tumorigenesis. Increasing our knowledge of proteome diversity regulated by different mtp53 proteins may translate into improved targets for clinical protocols designed for "triple-negative" breast cancers because 80% of such cancers express mtp53 (6). This could potentially include the use of PARP inhibitors as part of a synthetic lethal approach for the targeting of breast cancers that express mtp53 (34–36).

Materials and Methods

Reagents. Doxycycline, aprotinin, leupeptin, DTT, and trypan blue solution were obtained from Sigma, nonfat dry milk from Bio-Rad, Novex 4–12% Tris·glycine gradient gels from Life Technologies, and Vectashield mounting medium with DAPI from Fisher Scientific.

Cell Lines. MDA-MB-468, MDA-MB-231, T47D, and MCF-7, HT-29 cell lines were obtained from American Type Culture Collection and cultured in DMEM or McCoy (for HT-29) medium (Invitrogen), supplemented with 10% FBS (Gemini) and 50 U/mL penicillin and 50 μg/mL streptomycin (Mediatech). Cell lines with the inducible p53 knockdown were generated and described previously (3, 18, 37). To induce shRNA expression, cells were treated with 8 μg/mL doxycycline (2 μg/mL for MCF-7) for the time periods indicated in the figure legends, and fresh medium with doxycycline was supplemented every 48 h.

Antibodies. Anti-human p53 mouse 1:1:1 mix of hybridoma supernatants pAb421, pAb240, and pAb1801 (N terminus, central, and C terminus regions, respectively) and rabbit anti-Actin were obtained from Sigma. Mouse anti-PARP was obtained from BD Biosciences, rabbit anti-PAR from Calbiochem, rabbit anti-YAP1 and rabbit anti-MCM4 from Cell Signaling, mouse anti-PCNA PC10 from Abcam, mouse anti-Paxillin from Millipore, and mouse anti-Fibrillarin from Abcam. Secondary antibodies were as follows: anti-mouse and anti-rabbit HRP-conjugated (Sigma) and anti-rabbit Alexa Fluor 594-conjugated (Life Technologies).

Whole-Cell Protein Extracts. Cells were lysed in RIPA buffer (0. 1% SDS, 1% Nonidet P-40, 150 mM NaCl, 1 mM EDTA, 0.5 mM EGTA, 50 mM Tris·Cl, pH 8) with 1 mM PMSF, 8.5 μg/mL aprotinin, and 2 μg/mL leupeptin following standard protocol.

Subcellular Fractionation. Cells were harvested, and fractionation was performed by using the Stillman protocol (23). Briefly, after removing the media, cells were rinsed with cold PBS solution twice, scraped from the plates, and pelleted by centrifugation in 50-mL tubes at 91.7 × *g* for 5 min. Cell pellets were suspended in buffer A [10 mM Hepes, pH 7.9, 10 mM KCl, 1.5 mM $MgCl_2$, 0.34 M sucrose, 10% (vol/vol) glycerol, 1 mM DTT, 0.5 mM PMSF, 2 μg/mL leupeptin, 8.5 μg/mL aprotinin] with 0.1% Triton X-100. After 5 min incubation on ice, cells were spun down at 1,188 × *g* for 5 min at 4 °C. The supernatant was spun down for an additional 5 min at 15,493 × *g* at 4 °C to clarify (cytoplasmic fraction). Pellets were washed two times with buffer A by centrifugation at 1,188 × *g* for 5 min at 4 °C. Resuspended nuclear pellet in buffer B (3 mM EDTA, 0.2 mM EGTA, 0.5 mM PMSF, 2 μg/mL leupeptin, 8.5 μg/mL aprotinin) was incubated on ice for 30 min with vigorous vortexing every 5 min and spun down at 1,467 × *g* for 5 min at 4 °C. The supernatant was nuclear soluble proteins (S2 fraction), and the pellet, enriched in chromatin, was washed two times with buffer B, resuspended in buffer B, and sonicated three times for 30 s, followed by 30 s of rest on ice (P3 fraction). Samples were stored at −80 °C.

Gel Electrophoresis and Immunoblotting. Proteins were separated by using gradient 4–12% SDS/PAGE and transferred to a nitrocellulose membrane. The membrane was blocked in 5% nonfat milk solution in PBS solution/0.1% Tween 20 and probed overnight at 4 °C. Washes were done with PBS solution/0.1% Tween 20 solution. Secondary anti-mouse or anti-rabbit antibody (Sigma) was applied to the membrane for 1 h at room temperature, and the membrane was washed three times. Protein signal was visualized by chemiluminescence using the Super Signal Kit (Pierce) and detected after exposure for autoradiography to Hyblot CL films (Denville Scientific).

Quantitative Proteomics by SILAC MS. For SILAC MS, we used Protein Quantitation Kit–DMEM (no. 89983; Pierce) with $^{13}C_6$ L-Lysine-2HCl and added to the media a second amino acid, $^{13}C_6$ $^{15}N_4$ L-Arginine-HCl (no. 89990; Pierce), for double labeling. Cells were passaged for at least five cell doublings by splitting cells when required, and isotope incorporation efficiency was determined by MS analysis. MDA-468.shp53 R273H depleted and nondepleted cells were cultured in media containing nonlabeled or labeled amino acids, harvested, and fractionated; cytoplasmic fractions were mixed at a 1:1 ratio, separated by SDS/PAGE, and stained with GelCode Blue Stain Reagent (Thermo Scientific); and 15 gel sections excised with in situ trypsin digestion of polypeptides in each gel slice was performed as described (38). The tryptic peptides were desalted by using a 2-μL bed volume of Poros 50 R2 reversed-phase beads (Applied Biosystems) packed in Eppendorf gel-loading tips (39). The purified peptides were diluted to 0.1% formic acid, and each gel section was analyzed separately by microcapillary LC with tandem MS by using the NanoAcquity system (Waters) with a 100-μm inner diameter × 10-cm length C18 column (1.7 μm BEH130; Waters) configured with a 180-μm × 2-cm trap column coupled to a Q-Exactive mass spectrometer (Thermo Fisher Scientific). Key parameters for the mass spectrometer were: automatic gain control (AGC) 3 × 106 ions, resolution 70,000. Tandem MS fragmentation spectra were searched for protein identification by using the Andromeda search engine (maxquant.org) against the reversed and concatenated IPI_HUMAN protein database (v3.87). One unique peptide was required for high-confidence protein identifications, and a minimum ratio count of two peptides (one unique and one razor) were required for SILAC ratio determination. Normalized SILAC ratios (i.e., H/L) were used for subsequent analysis. All MS/MS samples were analyzed by using MaxQuant (Max Planck Institute of Biochemistry; version 1.3.0.3) at default settings with a few modifications. The default was used for first search tolerance and main search tolerance: 20 ppm and 6 ppm, respectively. Labels were set to Arg10 and Lys6. MaxQuant was set up to search the reference human proteome database downloaded from UniProt April 2, 2013. MaxQuant performed the search assuming trypsin digestion with as many as two missed cleavages. Peptide, site, and protein FDR were all set to 1% with a minimum of one peptide needed for identification but two peptides needed to calculate a protein level ratio. The following modifications were used as variable modifications for identifications and included for protein quantification: oxidation of methionine, acetylation of the protein N terminus, and phosphorylation of serine, threonine, and tyrosine residues and propionamide for acrylamide adducts on cysteine. Raw data as well as original MaxQuant result files can be provided upon request.

Immunofluorescence. Cells on the coverslips were briefly rinsed with cold PBS solution, fixed in 4% formaldehyde for 15 min, and permeabilized in 0.5% Triton X-100 in PBS solution plus 1% milk for 10 min at room temperature. After three washes with PBS solution plus 1% milk, coverslips were incubated with primary antibody for 1 h at room temperature, washed three times, and then incubated in secondary antibody for 1 h at room temperature. After the last wash, coverslips were placed on a slide (cells faced down) into a drop of DAPI containing mounting media. Immunofluorescence was visualized by using an UltraVIEW ERS Spinning-Disk Microscope (PerkinElmer).

FACS. FACS was performed on a FACScan device (BD Biosciences). After treatments, cells were harvested, washed, resuspended in PBS solution containing 2% BSA and 0.1% sodium azide, fixed in 30% ethanol, and stored overnight at 4 °C. Before sorting, propidium iodide staining and RNase treatment were performed for 30 min at 37 °C.

Quantitative RT-PCR. RNA was isolated by using QIAshredder columns and RNeasy Mini Kit (Qiagen). A total of 5 μg of RNA was used for cDNA synthesis by using High Capacity cDNA Archive Kit reagents (Applied Biosystems). A total of 150 ng of cDNA was combined with TaqMan Universal Master Mix (Applied Biosystems) and Applied Biosystems Assays on Demand primers/probes for *PCNA* (Hs00427214_g1), *MCM4*(Hs00907398_m1), *p53*(Hs00153340_m1), or *GAPDH* (433764-1207037). The PCR was carried out on a 7500 Sequence Detection System (Applied Biosystems) as follows: one cycle, 2 min (50 °C); one cycle, 10 min (94 °C); and 40 cycles, 15 s (94 °C) and 1 min (60 °C).

RNAi and Transfections. For siRNA experiments, HT-29 cells were seeded at 60% confluence in media without penicillin–streptomycin and allowed to attach overnight. Cells were transfected with 100 nM of *p53* or nontargeted siRNA Smart Pool (Dharmacon) for 6 h by using Lipofectamine 2000 (Invitrogen) per manufacturer's protocol. At the end of the incubation period, an equal volume of McCoy media with 40% FBS was added, and the next morning fresh media with 10% FBS was added and the cells were allowed to grow for 72 h.

ACKNOWLEDGMENTS. We thank John Philip for the MaxQuant analysis, Hediye Erdjument-Bromage for the gel digestion and Mascot analysis, and Amy Zhong for the art for Figs. 2*A* and 7. This work was supported by a grant from the Breast Cancer Research Foundation (to J.B.) and National Institutes of Health (NIH)/National Cancer Institute Cancer Center Support Grant P30 CA08748 to the Microchemistry and Proteomics Core Laboratory, Memorial Sloan–Kettering Cancer Center (to R.C.H.). Hunter College infrastructure was supported by Grant MD007599 from the National Institute on Minority Health and Health Disparities of the NIH.

1. Perou CM, et al. (2000) Molecular portraits of human breast tumours. *Nature* 406(6797):747–752.
2. Muller PA, Vousden KH (2013) p53 mutations in cancer. *Nat Cell Biol* 15(1):2–8.
3. Freed-Pastor WA, et al. (2012) Mutant p53 disrupts mammary tissue architecture via the mevalonate pathway. *Cell* 148(1-2):244–258.
4. Freed-Pastor WA, Prives C (2012) Mutant p53: One name, many proteins. *Genes Dev* 26(12):1268–1286.
5. Powell E, Piwnica-Worms D, Piwnica-Worms H (2014) Contribution of p53 to metastasis. *Cancer Discov* 4(4):405–414.
6. Cancer Genome Atlas Network (2012) Comprehensive molecular portraits of human breast tumours. *Nature* 490(7418):61–70.
7. Levine AJ, Oren M (2009) The first 30 years of p53: Growing ever more complex. *Nat Rev Cancer* 9(10):749–758.
8. Brosh R, Rotter V (2009) When mutants gain new powers: News from the mutant p53 field. *Nat Rev Cancer* 9(10):701–713.
9. Suh YA, et al. (2011) Multiple stress signals activate mutant p53 in vivo. *Cancer Res* 71(23):7168–7175.
10. Muller PA, Vousden KH (2014) Mutant p53 in cancer: New functions and therapeutic opportunities. *Cancer Cell* 25(3):304–317.
11. Lang GA, et al. (2004) Gain of function of a p53 hot spot mutation in a mouse model of Li-Fraumeni syndrome. *Cell* 119(6):861–872.
12. Olive KP, et al. (2004) Mutant p53 gain of function in two mouse models of Li-Fraumeni syndrome. *Cell* 119(6):847–860.
13. Brázdová M, et al. (2013) Preferential binding of hot spot mutant p53 proteins to supercoiled DNA in vitro and in cells. *PLoS ONE* 8(3):e59567.
14. Coffill CR, et al. (2012) Mutant p53 interactome identifies nardilysin as a p53R273H-specific binding partner that promotes invasion. *EMBO Rep* 13(7):638–644.
15. Rivlin N, et al. (2014) Rescue of embryonic stem cells from cellular transformation by proteomic stabilization of mutant p53 and conversion into WT conformation. *Proc Natl Acad Sci USA* 111(19):7006–7011.
16. Shiio Y, et al. (2003) Quantitative proteomic analysis of chromatin-associated factors. *J Am Soc Mass Spectrom* 14(7):696–703.
17. Chou DM, et al. (2010) A chromatin localization screen reveals poly (ADP ribose)-regulated recruitment of the repressive polycomb and NuRD complexes to sites of DNA damage. *Proc Natl Acad Sci USA* 107(43):18475–18480.
18. Rodriguez OC, et al. (2012) Dietary downregulation of mutant p53 levels via glucose restriction: Mechanisms and implications for tumor therapy. *Cell Cycle* 11(23):4436–4446.
19. Shi M, Shtraizent N, Polotskaia A, Bargonetti J, Matsui H (2014) Impedimetric detection of mutant p53 biomarker-driven metastatic breast cancers under hyposmotic pressure. *PLoS ONE* 9(6):e99351.
20. Nigro JM, et al. (1989) Mutations in the p53 gene occur in diverse human tumour types. *Nature* 342(6250):705–708.
21. Bargonetti J, Friedman PN, Kern SE, Vogelstein B, Prives C (1991) Wild-type but not mutant p53 immunopurified proteins bind to sequences adjacent to the SV40 origin of replication. *Cell* 65(6):1083–1091.
22. Bargonetti J, Reynisdóttir I, Friedman PN, Prives C (1992) Site-specific binding of wild-type p53 to cellular DNA is inhibited by SV40 T antigen and mutant p53. *Genes Dev* 6(10):1886–1898.
23. Méndez J, Stillman B (2000) Chromatin association of human origin recognition complex, cdc6, and minichromosome maintenance proteins during the cell cycle: Assembly of prereplication complexes in late mitosis. *Mol Cell Biol* 20(22):8602–8612.
24. Krishnakumar R, et al. (2008) Reciprocal binding of PARP-1 and histone H1 at promoters specifies transcriptional outcomes. *Science* 319(5864):819–821.
25. Beneke S (2012) Regulation of chromatin structure by poly(ADP-ribosyl)ation. *Front Genet* 3:169.
26. Subramanian A, et al. (2005) Gene set enrichment analysis: A knowledge-based approach for interpreting genome-wide expression profiles. *Proc Natl Acad Sci USA* 102(43):15545–15550.
27. Croft D, et al. (2014) The Reactome pathway knowledgebase. *Nucleic Acids Res* 42(Database issue):D472–D477.
28. Sonnenblick A, de Azambuja E, Azim HA, Jr, Piccart M (2015) An update on PARP inhibitors-moving to the adjuvant setting. *Nat Rev Clin Oncol* 12(1):27–41.
29. Murray J, et al. (2014) Tumour cell retention of rucaparib, sustained PARP inhibition and efficacy of weekly as well as daily schedules. *Br J Cancer* 110(8):1977–1984.
30. García-Parra J, et al. (2014) Poly (ADP-ribose) polymerase inhibition enhances trastuzumab antitumour activity in HER2 overexpressing breast cancer. *Eur J Cancer* 50(15):2725–2734.
31. Polotskaia A, et al. (2012) 8-Amino-adenosine activates p53-independent cell death of metastatic breast cancers. *Mol Cancer Ther* 11(11):2495–2504.
32. Lonskaya I, et al. (2005) Regulation of poly(ADP-ribose) polymerase-1 by DNA structure-specific binding. *J Biol Chem* 280(17):17076–17083.
33. Rausch T, et al. (2012) Genome sequencing of pediatric medulloblastoma links catastrophic DNA rearrangements with TP53 mutations. *Cell* 148(1-2):59–71.
34. Javle M, Curtin NJ (2011) The role of PARP in DNA repair and its therapeutic exploitation. *Br J Cancer* 105(8):1114–1122.
35. Turner NC, et al. (2008) A synthetic lethal siRNA screen identifying genes mediating sensitivity to a PARP inhibitor. *EMBO J* 27(9):1368–1377.
36. Hastak K, Alli E, Ford JM (2010) Synergistic chemosensitivity of triple-negative breast cancer cell lines to poly(ADP-ribose) polymerase inhibition, gemcitabine, and cisplatin. *Cancer Res* 70(20):7970–7980.
37. Brekman A, Singh KE, Polotskaia A, Kundu N, Bargonetti J (2011) A p53-independent role of Mdm2 in estrogen-mediated activation of breast cancer cell proliferation. *Breast Cancer Res* 13(1):R3.
38. Sebastiaan Winkler G, et al. (2002) Isolation and mass spectrometry of transcription factor complexes. *Methods* 26(3):260–269.
39. Erdjument-Bromage H, et al. (1998) Examination of micro-tip reversed-phase liquid chromatographic extraction of peptide pools for mass spectrometric analysis. *J Chromatogr A* 826(2):167–181.